



HAL
open science

Spatial analysis of the La paca, SE spain, 2005 seismic series through the relative location of multiplets and principal component analysis

E. Ocaña, D. Stich, E. Carmona, F. Vidal, M. Bretón, M. Navarro, A. García-Jerez

► To cite this version:

E. Ocaña, D. Stich, E. Carmona, F. Vidal, M. Bretón, et al.. Spatial analysis of the La paca, SE spain, 2005 seismic series through the relative location of multiplets and principal component analysis. *Physics of the Earth and Planetary Interiors*, 2008, 166 (3-4), pp.117. 10.1016/j.pepi.2007.12.005 . hal-00532134

HAL Id: hal-00532134

<https://hal.science/hal-00532134>

Submitted on 4 Nov 2010

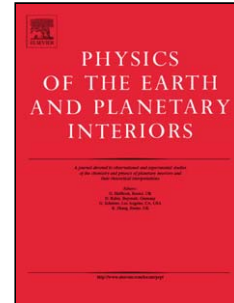
HAL is a multi-disciplinary open access archive for the deposit and dissemination of scientific research documents, whether they are published or not. The documents may come from teaching and research institutions in France or abroad, or from public or private research centers.

L'archive ouverte pluridisciplinaire **HAL**, est destinée au dépôt et à la diffusion de documents scientifiques de niveau recherche, publiés ou non, émanant des établissements d'enseignement et de recherche français ou étrangers, des laboratoires publics ou privés.

Accepted Manuscript

Title: Spatial analysis of the La paca, SE Spain, 2005 seismic series through the relative location of multiplets and principal component analysis

Authors: E. Ocaña, D. Stich, E. Carmona, F. Vidal, M. Bretón, M. Navarro, A. García-Jerez



PII: S0031-9201(08)00027-7
DOI: doi:10.1016/j.pepi.2007.12.005
Reference: PEPI 4895

To appear in: *Physics of the Earth and Planetary Interiors*

Received date: 7-6-2007
Revised date: 28-9-2007
Accepted date: 3-12-2007

Please cite this article as: Ocaña, E., Stich, D., Carmona, E., Vidal, F., Bretón, M., Navarro, M., García-Jerez, A., Spatial analysis of the La paca, SE Spain, 2005 seismic series through the relative location of multiplets and principal component analysis, *Physics of the Earth and Planetary Interiors* (2007), doi:10.1016/j.pepi.2007.12.005

This is a PDF file of an unedited manuscript that has been accepted for publication. As a service to our customers we are providing this early version of the manuscript. The manuscript will undergo copyediting, typesetting, and review of the resulting proof before it is published in its final form. Please note that during the production process errors may be discovered which could affect the content, and all legal disclaimers that apply to the journal pertain.

1 SPATIAL ANALYSIS OF THE LA PACA, SE SPAIN, 2005 SEISMIC SERIES
2 THROUGH THE RELATIVE LOCATION OF MULTIPLETS AND
3 PRINCIPAL COMPONENT ANALYSIS

4 E. Ocaña^{a*}, D. Stich^{b1}, E. Carmona^a, F. Vidal^{a,c}, M. Bretón^d, M. Navarro^{a,e} and A. García-Jerez^e

5
6 ^aInstituto Andaluz de Geofísica, Universidad de Granada. 18071 Granada, Spain.

7 ^bIstituto Nazionale di Geofisica e Vulcanologia, Sezione di Bologna. 40128 Bologna, Italy.

8 ^cDepartamento de Física Teórica y del Cosmos, Universidad de Granada. 18071 Granada, Spain.

9 ^dObservatorio Vulcanológico, Universidad de Colima. 28045 Colima, México.

10 ^eDepartamento de Física Aplicada, Universidad de Almería. 04120 Almería, Spain.

11

12

13

14 **Abstract**

15

16 On January 29 2005, an M_W 4.8, I_{max} VI-VII, earthquake occurred near the village of
17 La Paca, SE Spain. The aftershock sequence shows distinct heterogeneity, manifested
18 in a non-uniform temporal decay of activity and different source mechanisms for the
19 main shock and the largest aftershocks. We analysed 262 earthquakes of the seismic
20 series in order to characterize the active seismic structures. Moving-window cross-
21 correlation of the P- and S-waveforms recorded at local broad-band stations and the
22 application of a selection algorithm have allowed to identify events with similar
23 waveforms (multiplets) and to classify them into 16 clusters of 3 to 25 earthquakes
24 each. In each multiplet cluster, events have been relocated with respect to a master
25 event by the linear inversion of cross-correlation time lags for P and S-waves.

* Corresponding author. Fax: +34 958 160907

E-mail address: elena@iag.ugr.es (E. Ocaña)

¹ Now at Instituto Andaluz de Geofísica. Universidad de Granada. Spain.

26 Clusters show epicentral alignments with a predominant direction N145°E and two
27 secondary directions: N6°E and N40°E. Spatio-temporal patterns of the seismicity
28 have been analysed using Principal Component Analysis (PCA), upon the relocated
29 epicentre distribution and we have obtained three trends, N42°E, N14°E and N145°E,
30 present during all the sequence. These directions inferred from relative location and
31 PCA are coincident with nodal planes of moment tensor solutions for the larger
32 events within the series. They can be interpreted as the simultaneous activity of
33 conjugate strike-slip faults under a N160°-170°E orientation of the principal
34 compressive stress σ_1 .

35

36

37 **Keywords:** seismic series, multiplet analysis, master-event relative location, Principal
38 Component Analysis.

39

40

41 **Introduction**

42

43 Retrieving the precise spatial distribution of tightly clustered earthquakes within a
44 seismic series can help to image fault zone geometry and to associate seismic activity
45 to a particular tectonic structure. Such results may provide important constraints to
46 understand regional seismotectonics, and resolve the ambiguity between fault and
47 auxiliary plane for point-source focal mechanisms. When the inter-spacing between
48 clustered events is of the same order or less than single event location errors, the
49 spatial distribution cannot be resolved by routine location procedures anymore.
50 However, a more accurate location of them can be achieved through a relative

51 location approach, such as joint hypocenter determination (Douglas, 1967), the
52 double difference technique (Waldhauser and Ellsworth, 2000) or the master event
53 technique (e.g. Fitch, 1975). Furthermore, events originated along a single fault patch
54 commonly generate similar ground motion at a seismic recording station, as they have
55 similar source radiation patterns and nearby propagation paths through the
56 heterogeneous earth (Geller and Mueller, 1980; Deichmann and García-Fernández,
57 1992). Those events with nearly identical waveforms are commonly referred to as
58 doublets (if there is a pair of events) or multiplets (if there are more than two similar
59 events). For seismic multiplets, we can exploit the waveform similarity to obtain an
60 accurate relative timing of P- and S-phases between the different earthquakes by
61 waveform cross-correlation or cross-spectral analysis of the respective arrivals (e.g.
62 Scherbaum and Wendler, 1986), permitting a precise relative location with standard
63 errors often in the range of a few tens of meters only. Such approaches are now
64 frequently applied to resolve the seismotectonic fine structure in areas of intense local
65 seismicity (recent studies e.g. by Scarfi et al., 2003; Moriya et al., 2003; Alparone
66 and Gambino, 2003; Hemmann et al., 2003; Hurukawa et al., 2003; Schaff et al.,
67 2004; Hauksson and Shearer, 2005; Mandal et al., 2006; Kraft et al., 2006; Massa et
68 al., 2006; Ruiz et al., 2006).

69
70 Southern Spain shows a moderate level of seismicity in the context of oblique
71 Eurasian-Nubian plate convergence at a rate of ~ 5 mm/year (McClusky et al., 2003;
72 Serpelloni et al., 2007) as well as coeval extensional tectonics related to the formation
73 of the Alboran Basin and Neogene intramountain basins in the Betic Cordillera
74 (Lonergan and White, 1997; Galindo-Zaldívar, 1999). The complicated geodynamic
75 setting is reflected in a widespread, diffuse distribution of earthquakes (Fig. 1) and

76 heterogeneous patterns in the orientation and faulting style of earthquake source
77 mechanisms (Vidal, 1986; Buforn et al. 2004; Stich et al., 2006). An important
78 portion of the seismic activity occurs within seismic series, including both
79 (foreshock)-mainshock-aftershock sequences and extensive seismic swarms without a
80 single dominating mainshock. Examples include the 1979 seismic series in the
81 Granada basin, with 55 felt earthquakes with magnitude m_d up to 4.8, which lasted
82 almost a year (Vidal, 1986), the 1985 seismic swarms near the town of Loja (~1500
83 earthquakes, $m \leq 3.9$, Posadas, 1991), the 1988-1989 Agrón seismic swarm (~400
84 earthquakes, $m \leq 4.0$, Saccorotti et al., 2002), the swarm occurred in the town of
85 Antequera in June 1989 (Posadas et al., 1993) containing 158 earthquakes with
86 magnitudes between 2.5 and 3.4, or the extensive aftershock sequence of the 1993-
87 1994, M_w 4.8 and 4.9 Adra-Berja earthquakes with ~500 events (Stich et al., 2001).
88
89 Here, we analyse a seismic series in January and February 2005 near the town of
90 Lorca, Murcia province, SE Spain. Following the M_w 4.8 mainshock on January 29
91 (Buforn et al., 2006; Cesca et al., 2006; Benito et al., 2007), important aftershock
92 activity with more than 400 earthquakes was lasting for more than two weeks. We are
93 interested in identifying the fault responsible for the main shock, which caused
94 significant damage in the epicentral area, and to investigate apparent heterogeneity in
95 the aftershock sequence, where a non-uniform temporal decay of the activity and
96 differences between the source mechanisms for the main shock and the largest
97 aftershocks suggest that two different rupture processes are involved (Benito et al.,
98 2007). We use data from seven three-component broad-band stations out to ~100 km
99 epicentral distance to perform (a) traditional single event relocation of the series, (b)
100 cross-correlation of P- and S- waveforms between events to identify similar

101 earthquakes in the series, (c) cluster analysis (Maurer and Deichmann, 1995) to
102 classify those similar earthquakes into groups or families of multiplet events, and (d)
103 relocation of each multiplet cluster relative to a master event, based on the arrival
104 time differences to each station between master and slaves as obtained from cross-
105 correlation. Multiplet relocations are interpreted directly, as well as through a
106 statistical analysis of their spatial and temporal distribution based in the Principal
107 Component Analysis (PCA) (Michelini and Bolt, 1986; Posadas, 1991; Posadas et al.,
108 1993; Saccorotti et al., 2002). Results are finally compared to the focal mechanisms
109 for the larger earthquakes of the sequence and interpreted and discussed in the light of
110 active tectonics in the area.

111

112

113 **The 2005 La Paca earthquake series**

114

115 The eastern termination of the Betic Cordilleras in SE Spain is characterized by
116 moderate seismic activity (Fig. 2). Historical records contain a number of relevant
117 earthquakes that caused serious damage, most notably the 1829 Torrevieja earthquake
118 in the province of Alicante ($I_{\max} = IX-X$, estimated magnitude $M_s = 6.9$, Muñoz and
119 Udías, 1991). The region of Murcia experienced a dozen earthquakes with magnitude
120 larger than 4 during instrumental times. Maximum intensity of VIII was reached for
121 two earthquakes in 1911 (near Torres de Cotillas and Lorquí, estimated magnitudes
122 M_s of 5.7 and 5.3, Buforn et al., 2005) and for the 1948 earthquake near Cehegin.
123 The following 50 years produced less significant earthquakes, but in the recent eight
124 years the region has experienced a notable succession of three seismic series: the first
125 of them began on 1999 February 2 and had a main shock of M_w 4.8 located near the

126 village of Mula, the second one started on 2002 August 6 close to the village of
127 Bullas with a M_w 5.0 event, and the third one occurred on 2005 January 29, M_w 4.8,
128 close to the village of La Paca. The three shocks had shallow focii and predominately
129 strike-slip focal mechanisms (Mancilla et al., 2002; Martínez-Díaz et al., 2002; Stich
130 et al., 2003; Buforn et al., 2005; Buforn et al., 2006; Cesca et al., 2006; Stich et al.,
131 2006; Benito et al., 2007).

132

133 The M_w 4.8 earthquake on 2005 January 29 (07:41:31) marked the beginning of the
134 seismic series studied. The main shock was felt with a maximum intensity of VII and
135 VI-VII (EMS 98) in La Paca and Zarçilla de Ramos close to the epicentre, causing
136 surprisingly high damage for an event of this magnitude (Buforn et al., 2006; Benito
137 et al., 2007). Several aftershocks were also felt by the population (January 29
138 (08:10:57, M_w 3.6), February 3 (11:40:33, M_w 4.2) and February 4 (01:09:41, M_w
139 3.9)). The seismic activity decreased from January 29 until February 3, when the M_w
140 4.2 shock drove up the rate of activity with 76 events recorded that day and 61
141 recorded on February 4 (Fig. 3), followed by a large number of aftershocks. While the
142 overall evolution of the series appears complex, each of the two peaks alone satisfies
143 Omori's law for the temporal decay of activity and the Gutenberg-Richter relation for
144 the magnitude–frequency distribution, yielding b-value-estimates of 0.64 and 0.9
145 respectively (Benito et al., 2007). The duplication of patterns in the aftershock
146 sequence and different moment tensor mechanisms for the main shock and largest
147 aftershocks (Fig. 4) suggest that (at least) two different rupture processes are active
148 during the seismic series.

149

150 For our study, we selected events that occurred between longitude 2.4° – 1.2° W and
151 latitude 37.3° – 38.3° N, during the three-week period (from January 29 to February 20)
152 of maximum activity in the series, from the seismic catalogue of the Instituto Andaluz
153 de Geofísica. The initial date of our analysis coincides with the day when series
154 started whereas the final date, February 20, was fixed taking into account that from
155 that day the seismic activity clearly decreases and only sparse events occur (Fig. 3).
156 With these criteria, 262 earthquakes were selected, with magnitudes between 1.2 and
157 4.8. For these earthquakes, we collected waveforms from seven seismic stations close
158 to the epicentral area (~ 30 km to ~ 100 km distance, Fig. 4), which were operating
159 during the sequence (ACLR, ASCB, SESP and VELZ from Instituto Andaluz de
160 Geofísica, EMUR and ETOB from Instituto Geográfico Nacional, and CART from
161 GEOFON/Real Observatorio de la Armada/Universidad Complutense). All of them
162 are three-component broad-band stations and they offer a good azimuthal coverage of
163 the earthquakes. We carefully hand-picked P- and S- arrivals in the seismograms, and
164 obtained first hypocentral determinations for the 2005 series from single-event
165 relocation (Hypocenter, Lienert and Haskov, 1995). The new locations group most of
166 the seismicity very close to the main shock (Fig. 4), with most of the events located in
167 the upper crust and showing a tendency to line up in approximately NW-SE direction.
168 The main shock (37.84° N, 1.80° W) was relocated 5.5 km from the epicentre given by
169 the Instituto Geográfico Nacional (37.88° N, 1.78° W) in the immediate proximity of
170 Zarcilla de Ramos and La Paca, consistent with the highest macroseismic intensities
171 observed there (Buforn et al., 2006; Benito et al., 2007). The difference in both
172 locations reflects the different coverage of stations and velocity model used in our
173 study.
174

175

176 **Multiplet detection**

177

178 Events with very similar waveforms at the same recording station are expected to be
179 tightly clustered (Geller and Mueller, 1980), and are suitable for the relocation
180 approach adopted in this study. In order to identify pairs of closely spaced
181 earthquakes, a normalized moving-window cross-correlation analysis between pairs
182 of seismograms was performed (Stich et al., 2001; Saccorotti et al., 2002; Kraft et al.,
183 2006; Ruiz et al., 2006). The similarity between two waveforms was quantified as the
184 maximum value of the cross-correlation coefficient, and the corresponding time lag
185 of the traces was stored to obtain relative locations later on. Though multiplets should
186 exhibit waveform similarity at all stations of a network, we decided to base multiplet
187 detection in the single station VELZ, the closest one to the epicentral area, because it
188 provides clearly the best signal-to-noise ratio for the smaller earthquakes of the series.
189 We used time windows of length 2s starting 0.5s before our picked P and S onsets,
190 and applied a bandpass filter between 1 Hz and 15 Hz. P-wave correlations were
191 measured on the vertical component, and S-wave correlations on the horizontal
192 components. Window length and filter band were adjusted by trial and error by
193 evaluating the performance in the following cluster analysis.

194

195 To classify similar earthquakes into clusters or families of multiplets, we use
196 equivalence class sorting (Press et al., 1992). It achieves its purpose by establishing
197 that if element A is similar to B and B is similar to C, then all the three elements A, B
198 and C are assigned to the same cluster. Aster and Scott (1993) introduced the method
199 to multiplet detection, regarding as similar elements two earthquakes that exceed two

200 chosen threshold values imposed to the P-wave similarity (T_P) and to the S-wave
201 similarity (T_S). A shortcoming of equivalence class sorting is that a single pair of
202 similar elements is sufficient to collapse two formerly independent clusters into a
203 single large one, even if other elements in the cluster show little similarity, which
204 makes the fine-tuning of threshold values critical. We use the algorithm developed by
205 Maurer and Deichmann (1995), which introduces a third threshold value named the
206 cluster separation threshold (T_{SP}), to stabilize the cluster classification. It is imposed
207 to the normalized scalar product of the corresponding rows of the S wave cross-
208 correlation matrix, thus assuring that similar elements show similar trends in their
209 cross-correlations with all other events inside and outside the cluster, and that a high
210 level of similarity throughout the different elements of the same family is maintained.

211

212 We tested different values of these thresholds until finding a reasonable compromise
213 ($T_P=0.7$, $T_S=0.8$, $T_{SP}=0.5$) between a possibly large number of clustered events and
214 a high waveform similarity within all individual clusters. Not counting doublets, we
215 obtained 16 clusters, composed of 3 to 25 multiplets (Fig. 5). They include a total of
216 118 earthquakes, 45% of the initial data set. Nearly all the clustered earthquakes
217 occurred in the first ten days after the mainshock, following the evolution of activity
218 over the seismic series. The first six clusters initiate within 24 hours after the first
219 earthquake. A second phase of activity of seven clusters, starting within 24 hours
220 after the second largest earthquake (M_W 4.2) on February 3, groups a higher number
221 of earthquakes and contains the largest clusters no. 17 and 23 (25 and 23 events,
222 respectively). The two largest aftershocks on February 3 and 4 show very similar
223 waveform and are grouped together in cluster no. 8, starting shortly after the
224 mainshock. At this stage, we also define absolute cluster locations, as a reference for

225 the relative location procedure, and to make another step towards a better spatial
226 characterization of the series. Assuming that cluster extensions are small compared to
227 the single-event location errors, we calculate absolute locations as the mean location
228 of all multiplet events included in each cluster, thus averaging out random errors of
229 the single locations (Fig. 6). Clusters group tightly around the mainshock and more
230 than half of them are located less than 5 km away. An example for waveform
231 similarity in a multiplet cluster (no. 3) is shown in Fig. 7.

232

233

234 **Relative location of multiplets**

235

236 Relative location of two events can be determined by P and S-wave arrival-time
237 differences to a given station, which are explained by origin time difference and
238 travel-times differences as waves travel along different length propagation paths. For
239 each cluster, a master event has been chosen based on the signal-to-noise ratio of
240 waveforms, and all other events (slaves) are located relative to it. For a pair of
241 master-slave events with very similar waveforms, we can take advantage of that
242 similarity to define highly accurate relative time delays from the time lag of their
243 cross-correlation maxima. A polynomial interpolator was applied to resample the
244 cross-correlation function for waveforms with different sampling rate (100/s at ETOB
245 and EMUR, 50/s at ACLR, ASCB, SESP and VELZ and 20/s at CART), which
246 allows estimating the position of the maximum with a formal precision about one
247 order of magnitude beyond the original sampling rates. To obtain a common base line
248 for all relative arrival times for a master-slave pair, the time lags were referenced to

249 the zero-lag position of the correlation windows and the GPS times of the first
 250 samples in the seismograms.

251

252 Assuming that the hypocentral separation between multiplet earthquakes is small
 253 compared to the event-station distance, all ray-paths between the source volume and a
 254 common receiver are similar and leave the source volume practically parallel to each
 255 other. For parallel rays, arrival-time differences between master and slave at a given
 256 station depend linearly on the spatial offset between the two sources, and can be
 257 expressed by the origin time difference and the projection of relocation vector \mathbf{f} on the
 258 direction \mathbf{n} of the ray leaving the source volume:

$$259 \quad \Delta t = \Delta T_0 - \frac{\mathbf{f} \cdot \mathbf{n}}{V} \quad (1)$$

260 where \mathbf{n} is the unit vector in the direction of the ray to the given station and v is the
 261 phase velocity at the cluster location of either P- or S-waves. This further implies the
 262 assumptions that P- and S-wave velocities are constant in the entire source volume of
 263 the cluster and during the period of occurrence of the multiplets. Strictly spoken, the
 264 changes in the stress field will probably change the velocity fields during observation,
 265 but such variations have been found to be small elsewhere (velocity variations and
 266 multiplets are treated in Poupinet et al., 1984; Haase et al., 1995). From m available
 267 time differences of P and S-phases to different stations, a system of m linear
 268 equations is set up, and four unknowns can be determined: the three components of
 269 the relocation vector (Δx , Δy , Δz) and the difference in origin time. The elements of
 270 the forward matrix connecting data and model parameters depend on the velocity
 271 model, cluster location and station geometry. Take-off angles and ray vectors \mathbf{n} were
 272 computed through ray tracing in a simple velocity model, consisting of a 2-km-thick
 273 layer ($v_p=5.4$ km/s, $v_s=3.1$ km/s) over a half space ($v_p=6.1$ km/s, $v_s=3.5$ km/s). The

274 problem of matrix inversion and model parameter determination was solved in a
275 least-squares sense by singular value decomposition (Press et al., 1992). Errors of
276 model parameters are described by the model covariance matrix that –in its diagonal
277 form– gives us the orientation and the lengths of the principal error axes of the square
278 standard deviations of the data (e.g. Lay and Wallace, 1996).

279

280 Examples of relocation of multiplets (clusters no. 17, 9 and 5) are plotted in Fig. 8.
281 The by far largest axis of the error ellipsoid coincides approximately with the z-
282 direction, representing vertical relocation error. Due to the recording geometry (the
283 closest station is 32 km from the main shock) depth resolution is low (errors reach the
284 order of kilometres) and will not be interpreted in this study. Relocated multiplets
285 show very tight clustering of the epicentre distributions with typical horizontal
286 dimension of about 500 m. Evidently, multiplet relocations collapse strongly in the
287 vicinity of the average cluster location, compared to the distribution of the same
288 earthquakes before being relocated, as is shown in panels (a) and (b) of Fig. 9,
289 respectively.

290

291 Multiplets within a cluster are commonly expected to originate on the same fault
292 plane to explain the coherency of seismograms. The local directions of those faults
293 can be determined by fitting a plane to the relocated multiplet hypocentres within
294 each cluster. The best-fitting planes were defined to minimise the L1-norm of
295 distances of the relocated events to that plane (Stich et al., 2001). Dip directions are
296 practically vertical (near 90°) but this is an artificial and unrealistic prolongation of
297 the clusters in vertical direction due to the large scatter of the relocated events in
298 depth. Azimuth values reveal a predominant trend with an average direction of

299 N145°±17°E which approximately corresponds to lineaments defined by clusters
300 number 7, 17, 23, 31 and 36. This trend is considered the most important one as it
301 represents 53% of the relocated multiplets. There are also two secondary groups of
302 epicentre lineaments with approximate directions N6°±6°E (clusters number 8, 9, 21
303 and 28, which include 20% of the relocated multiplets) and N40°±7°E (clusters
304 number 3, 4, 5 and 35, which include 17% of the relocated multiplets) (Table 1 and
305 Fig. 10). Two of the clusters (no. 17 - Fig.8 - and no. 23) appear to show both NW-SE
306 and SE-NW subtrends, suggesting that they image intersections of both fault systems.

307

308

309 **Principal Component Analysis**

310

311 Principal Component Analysis (PCA) is a multivariant statistical method for reducing
312 multidimensionality of a data set to a lower dimension. PCA has been applied here to
313 the characterization of a system of active faults from our relocated hypocenters of
314 earthquakes, in order to determine the local rupture ellipsoid and to retrieve the main
315 planes along which earthquakes occurred (Michelini and Bolt, 1986; Posadas, 1991;
316 Posadas et al., 1993). PCA represents a more general approach towards the
317 identification and quantification of spatial trends, and differs from our previous
318 interpretation in two other aspects. First, it takes into account the temporal occurrence
319 of events and their proximity in time. Second, it was applied to the entire set of
320 relocated multiplets instead of single clusters only, that is, it considers the multiplet
321 distribution within clusters as well as the relative locations between clusters (Fig. 9b),
322 which were obtained by collapsing the single event locations to their mean value (see

323 above). It thus merges two types of relative hypocenter locations with different
 324 accuracy, which we have to keep in mind when interpreting the results.

325

326 The point of departure for PCA is a set of N events written in a matrix form, whose
 327 rows are the earthquakes and whose columns contain hypocentral information relative
 328 to those earthquakes. The coordinates of hypocenters are used to define a scatter
 329 matrix S, whose elements are given by Cooley and Lohnes (1971):

$$330 \quad S_{im} = \frac{1}{K} \sum_{j=1}^K (x_{ji} - X_{0i})(x_{jm} - X_{0m}) \quad i, m = 1, 2, 3 \quad (3)$$

331 where j is the event number, and x are the spatial coordinates of the hypocenters with
 332 the subscripts (i, m) taking values of 1, 2 and 3 corresponding to longitude, latitude
 333 and depth, respectively. X_0 are calculated by:

$$334 \quad X_{0m} = \frac{1}{K} \sum_{j=1}^K x_{jm} \quad m = 1, 2, 3 \quad (4)$$

335 and represent the arithmetic average of the three Cartesian coordinates of the
 336 hypocenter. The scatter matrix is diagonalized, giving as eigenvectors the axes of an
 337 ellipsoid which best least-square fits the original cloud of hypocenters, and the length
 338 of these axes as the positive square roots of the eigenvalues λ_m . As this ellipsoid
 339 determines the fracture planes associated to earthquakes, Michelini and Bolt (1986)
 340 called it Local Rupture Ellipsoid (LRE). If the ratio between the largest and the
 341 smallest eigenvalue is less than 2.5, the LRE will be considered volumetric and will
 342 be rejected, else the two largest eigenvectors are assumed to define the rupture plane
 343 (Posadas, 1991).

344

345 To infer the evolution of the rupture process in time, the scatter matrix (S_{im}) is
 346 constructed by using subsets of K earthquakes, in temporal order of their occurrence.

347 A sliding window of K events is displaced along the whole set of earthquakes. We
 348 begin with the first one and take the following $K-1$, so if there is a set of N events, a
 349 total of $N-K+1$ LRE's will be available. The optimal value of K is that which makes
 350 the function $Q(N,K)$ constant (Ebblin and Michelini, 1986)

$$351 \quad Q(N, K) = (N - K + 1)^{-1} \sum_{q=1}^{N-K+1} \frac{\lambda_2^q(K)}{\lambda_3^q(K)} \quad (5)$$

352 where q is the number of the window and λ_2^q and λ_3^q are the average and the smallest
 353 eigenvalues, respectively. Here, the optimal length of the sliding window was chosen
 354 as $K=31$ (Fig. 11). This analysis provides information about the number of LRE's
 355 constructed through K time-consecutive earthquakes having a predominant planar
 356 structure.

357

358 The most relevant planes obtained from our spatio-temporal analysis of the rupture
 359 process are reported sequentially in Table 2. From Table 2 and the stereographic
 360 projection (Fig. 12) the process shows an evolution of the rupture characterized by
 361 three principal trends active during all the series: $N145^\circ \pm 3^\circ E$ (projections (a), (d) and
 362 (k)), $N42^\circ \pm 4^\circ E$ (projections (b), (e) and (f)) and $N14^\circ \pm 4^\circ E$ (projections (c), (g) to (i),
 363 (l) and (m)). The dominant trends determined by the PCA method are in excellent
 364 agreement with the three orientations, $N145^\circ E$, $N40^\circ E$ and $N6^\circ E$, obtained from
 365 fitting planes to individual multiplets.

366

367

368 **Conclusions**

369

370 We analysed the 2005 La Poca (Southeastern Spain) seismic series, using a total of
 371 262 earthquakes occurred during the three weeks posterior to the occurrence of the

372 M_w 4.8 main shock on January 29. Events have magnitudes from 1.2 to 4.8, and
373 single event location depths mainly in the range 0-15km. We identified similar
374 events, called multiplets, from moving-window cross-correlation analysis of
375 waveforms recorded at VELZ station. The similarity between waveforms was
376 quantified through the maximum cross-correlation, and events that exceed three
377 thresholds applied to P-wave similarity, S-wave similarity and the normalized scalar
378 product of the corresponding rows of the S-wave cross-correlation matrix were
379 grouped through an equivalence class analysis. 16 clusters with 3-25 elements were
380 detected, including nearly half of earthquakes involved in the analysis. Within each
381 multiplet cluster, relocations relative to a master event were calculated by linear
382 inversion of precise relative phase arrival times from cross-correlation analysis.
383 Relative epicentres were obtained with an accuracy less than a few hundreds of
384 metres whereas depth shows a higher uncertainty, with errors up to several
385 kilometres, due to the lack of observations at short epicentral distance. As a
386 consequence, dip values of the hypocenter distribution appear to be closer to 90° , and
387 restrict the interpretation to the epicentre distribution and lateral trends of seismicity.
388 The clear elongations of several multiplet clusters (Fig. 8) in fact suggest that most of
389 the seismicity occurs along rather steeply dipping planes.

390

391 We quantified relative epicentre alignments in two different ways. First, planes are fit
392 to the precise relocations within each individual multiplet, giving as the most relevant
393 trend a $N145\pm 17^\circ E$ orientation, and two more groups of clusters showing trends of
394 $N6^\circ\pm 6^\circ E$ and $N40^\circ\pm 7^\circ E$ (Table 1 and Fig. 10). Second, the spatio-temporal pattern of
395 the series is analysed through PCA, applied to the entire dataset of relocated
396 multiplets. Here, the most relevant trends inferred have azimuths $N145^\circ\pm 3^\circ E$,

397 N42°±4°E and N14°±4°E (Table2). An entirely independent piece of information
398 about the geometry of the seismic series is available from moment tensor source
399 mechanisms, which were obtained from inversion of three-component intermediate-
400 period seismograms at up to 12 near-regional stations (Stich et al., 2006, Benito et al.,
401 2007). The three multiplet directions (N145°E, N6°E and N40°E), as well as the three
402 main directions obtained from ACP (N145°E, N14°E and N42°E), are present in the
403 focal mechanisms of the three largest shocks, showing nodal planes with trends of
404 N132°E, N15°E, N11°E and N40°E (Table 3). This does not permit to identify the
405 fault plane of the main shock as both nodal planes appear in the multiplet directions,
406 but the excellent agreement from both types of analysis permits one to associate the
407 N145°E and N6°E or N40°E multiplet clusters with right-lateral and left-lateral strike-
408 slip faulting respectively (Fig. 13).

409

410 These sets of planes include acute angles towards North and South and kinematics
411 involving opposite sense of shear, which characterizes them as conjugate faults.
412 These faults form part of a major belt of distributed shear deformation that extends
413 from southeastern Spain over the Alboran Sea. The orientation of N349°E of the
414 maximum principal stress σ_1 in the shear belt (Stich et al., 2006) is close to the
415 bisecting line of the acute angle between the N145°E and the N6°E multiplet faults,
416 indicating a coincidence of local deformation and average regional stress conditions
417 (Fig. 13). From Fig. 5 we see that activity on patches of either direction occurs
418 simultaneously, a feature that has been occasionally identified in complex strike-slip
419 faulting sequences (e.g. Smith and Priestley, 2000; Hauksson et al., 2002). This
420 implies stress concentration at the intersection of the conjugate fault systems, which
421 can contribute to the intensity of the aftershock sequence. We finally note that

422 multiplet results for the 2005 series are different from our initial intuitive notion of
423 the spatio-temporal pattern: the two peaks in the seismicity evolution, accentuated by
424 the occurrence of larger earthquakes of different focal mechanism at the onset of each
425 peak, may appear consistent with a temporal succession of two different rupture
426 processes, but the multiplet assignment confirms that the presupposed second rupture
427 process is active from the very beginning of the series, and the presupposed first
428 rupture process does even account for the majority of events in the second burst of
429 activity.

430

431

432 **Acknowledgements**

433

434 We would like to thank the Instituto Geográfico Nacional (stations EMUR and
435 ETOB) and GEOFON Program (station CART) for making available waveforms used
436 in this study. We are very grateful to Editor George Helffrich and to two anonymous
437 reviewers whose comments have helped us to improve and enrich the manuscript. We
438 also appreciate the comments and suggestions proposed by Gerardo Alguacil. This
439 study has been supported by the CICYT, projects REN2003-08159-C02-02 and
440 CGL2007-66745-C02-01/BTE, and by the FPI program of the Spanish Ministry of
441 Education and Science.

442

443

444 **References**

445

- 446 Alparone, S., and Gambino, S., 2003. High precision locations of multiplets on south-
447 eastern flank of Mt. Etna (Italy): reconstruction of fault plane geometry. *Phys. Earth*
448 *Planet. Int.*, 135: 281-289.
- 449 Aster, R.C., and Scott, J., 1993. Comprehensive characterization of waveform
450 similarity in microearthquake datasets. *Bull. Seismol. Soc. Am.*, 4: 1307–1314.
- 451 Benito, B., Capote R., Murphy P., Gaspar-Escribano, J.M., Martínez-Díaz, J.J., Tsige,
452 M., Stich, D., García-Mayordomo, J., García Rodríguez, M.J., Jiménez, M.E., Insúa-
453 Arévalo, J.M., Álvarez-Gómez, J.A., and Canora, C., 2007. An Overview of the
454 Damaging and Low Magnitude *Mw* 4.8 La Paca Earthquake on 29 January 2005:
455 Context, Seismotectonics, and Seismic Risk Implications for Southeast Spain, *Bull.*
456 *Seism. Soc. Am.*, 97: 671-690.
- 457 Buforn, E., Bezzeghoud, M., Udías, A., and Pro, C., 2004. Seismic sources on the
458 Iberia-African plate boundary and their tectonic implications. *Pure appl. Geophys.*
459 161, 623-646.
- 460 Buforn, E., Benito, B., Sanz de Galdeano, C., del Fresno, C., Muñoz, D., and
461 Rodríguez, I., 2005. Study of the damaging earthquakes of 1911, 1999, and 2002 in
462 the Murcia, Southeastern Spain, region: Seismotectonic and seismic-risk implications.
463 *Bull. Seism. Soc. Am.* 95, 549-567.
- 464 Buforn, E., Cesca, S., Goded, T., del Fresno, C., and Muñoz, D., 2006. The Bullas
465 (Murcia, SE Spain) January 29, 2005 earthquake, *J. Seism.*, 10, 65–72.
- 466 Cattaneo, M., Augliera, P., Spallarossa, D., and Eva, C., 1997. Reconstruction of
467 seismogenetic structures by multiplet analysis: an example of western Liguria, Italy.
468 *Bull. Seismol. Soc. Am.*, 4: 971–986.
- 469 Cesca, S., Buforn, E., and Dahm, T., 2006. Amplitude spectra moment tensor

- 470 inversion of shallow earthquakes in Spain, *Geophys. J. Int.* 166, 839–854
- 471 Cooley, W.W., and Lohnes, P.P., 1971. *Multivariate data analysis*. John Wiley &
472 Sons, Inc. New York.
- 473 Deichmann, N., and García-Fernández, M., 1992. Rupture geometry from high-
474 precision relative hypocentre locations of microearthquake clusters. *Geophys. J. Int.*,
475 110: 501-517.
- 476 Douglas, A., 1967. Joint epicentre determination, *Nature*, 215, 47–48.
- 477 Ebblin, C., and Michelini, A., 1986. A principal parameters analysis of the aftershock
478 sequences applied to the 1977 Friuli, Italy, sequence. *Ann. Geophys.*, B, 4: 473-480.
- 479 Fitch, T.J., Compressional velocity in source regions of deep earthquakes: an
480 application of the master event technique. *Earth planet. Sci. Lett.*, 135, 156-166,
481 1975.
- 482 Galindo-Zaldivar, J., Jabaloy, A., Serrano, I., Morales, J., González-Lodeiro, F., and
483 Torcal, F., 1999. Recent and present-day stresses in the Granada Basin (Betic
484 Cordilleras): example of a late Miocene–present-day extensional basin in a
485 convergent plate boundary. *Tectonics* 18:686–702
- 486 Geller, R.J., and Mueller, C.S., 1980. Four similar earthquakes in Central California.
487 *Geophys. Res. Lett.*, 7: 821-824.
- 488 Haase, J.S., Shearer, P.M., and Aster, R.C., 1995. Constraints on temporal variations
489 in velocity near Anza, California, from analysis of similar event pairs. *Bull. Seismol.*
490 *Soc. Am.*, 85: 194–206.

- 491 Hauksson, E., Jones, L.M., and Hutton, K., 2002, The 1999 *M*_w 7.1 Hector Mine,
492 California, Earthquake Sequence: Complex Conjugate Strike-Slip Faulting, *Bull.*
493 *Seismol. Soc. Am.*, 92, 1154-1170.
- 494 Hauksson, E., and Shearer, P., 2005. Southern California hypocenter relocation with
495 waveform cross-correlation, part 1: results using the double-difference method. *Bull.*
496 *Seismol. Soc. Am.*, 95: 1353–1368.
- 497 Hemmann, A., Meier, T., Jentzsch, G., and Ziegert, A., 2003. Similarity of
498 waveforms and relative relocalisation of the earthquake swarm 1997/1998 near
499 Werdau. *J. Geodyn.*, 35: 191-208.
- 500 Hurukawa, N., Tsuji, Y., and Waluyo, B., 2003. The 1998 Papua New Guinea
501 earthquake and its fault plane estimated from relocated aftershocks. *Pure Appl.*
502 *Geophys.*, 160: 1829-1841.
- 503 Kraft, T., Wassermann, J., and Igel, H., 2006. High-precision relocation and focal
504 mechanisms of the 2002 rain-triggered earthquake swarms at Mt Hochstaufen, SE
505 Germany. *Geophys. J. Int.*, 167: 1513-1528.
- 506 Lay, T. and Wallace, T.C., 1996. *Modern global seismology*. Academic Press, San
507 Diego.
- 508 Lienert, B.R., and J. Haskov, 1995. A computer program for locating earthquakes
509 both locally and globally. *Seismological Research Letters*, 66, 26-36.
- 510 Lonergan, L. and White, N., 1997. Origin of the Betic-Rif mountain belt. *Tectonics*
511 16, 504-522.
- 512 Mancilla, F., Ammon, C.J., Herrmann, R.B., and Morales, J., 2002. Faulting
513 parameters of the 1999 Mula earthquake, southeastern Spain. *Tectonophysics*, 354:
514 139– 155.

- 515 Mandal, P., Narsaiah, R., Sairam, B., Satyamurty, C., and Raju, I.P., 2006. Relocation
516 of early and late aftershocks of the 2001 Bhuj Earthquake using Joint Hypocentral
517 Determination (JHD) technique: implication toward the continued aftershock activity
518 for more than four years. *Pure Appl. Geophys.*, 163: 1561-1581.
- 519 Martínez-Díaz, J.J., 1998. Neotectónica y Tectónica Activa del sector
520 centrooccidental de Murcia y Sur de Almería, Cordillera Bética (España). PhD thesis,
521 Complutense University of Madrid, Madrid, pp. 466.
- 522 Martínez-Díaz, J.J., Rigo, A., Louis, L., Capote, R., Hernández- Henrile, J., Carreño,
523 E., and Tsige, M., 2002, Caracterización geológica y sismotectónica del terremoto de
524 Mula (Febrero 1999, Mb 4.8) mediante la utilización de datos geológicos,
525 sísmológicos y de interferometría de RADAR (INSAR). *Geogaceta* 31, 157–160.
- 526 Massa, M., Eva, E., Spallarossa, D. and Eva, C., 2006. Detection of earthquake
527 clusters on the basis of waveform similarity: an application in the monferrato region
528 (Piedmont, Italy). *J. Seism.*, 10: 1-22.
- 529 McClusky, S., Reilinger, R., Mahmoud, S., Ben Sari, D., and Tealeb, A., 2003. GPS
530 constraints on Africa (Nubia) and Arabia plate motions. *Geophys. J. Int.*, 155, 126-
531 138.
- 532 Maurer, H., and Deichmann, N., 1995. Microearthquake cluster detection based on
533 waveform similarities, with an application to the western Swiss Alps. *Geophys. J. Int.*
534 123: 588–600.
- 535 Michelini, A., and Bolt, B.A., 1986. Application of the principal parameters method
536 to the Coalinga, California, aftershock sequence. *Bull. Seismol. Soc. Am.*, 76: 409-
537 420.
- 538 Muñoz, D., and Udías, A., 1991. Three large historical earthquakes in southern Spain.

- 539 In: Seismicity, Seismotectonics and Seismic Risk of the Ibero-Maghrebian Region.
540 Instituto Geográfico Nacional, Madrid, 175–182.
- 541 Posadas, A.M., 1991. Análisis espacio-temporal de series sísmicas. Aplicación a las
542 Béticas centrales. PhD thesis, University of Granada, Granada, 480 pp.
- 543 Posadas, A.M., Vidal, F., De Miguel, F., Alguacil, G., Peña, J., Ibáñez, J.M., and
544 Morales, J., 1993. Spatial-temporal analysis of a seismic series using the Principal
545 Components Method: the Antequera series, Spain, 1989. *J. Geophys. Res.*, 98: 1923-
546 1932.
- 547 Poupinet, G., Ellsworth, W.L., and Frechet, J., 1984. Monitoring velocity variations
548 in the crust using earthquakes doublets: an application to the Calaveras fault,
549 California. *J. Geophys. Res.*, 89: 5719–5731.
- 550 Press, W.H., Teukolsky, S.A., Vetterling, W.T., and Flannery, B.P., 1992. Numerical
551 Recipes: The Art of Scientific Computing, 2nd Edition. Cambridge University Press,
552 Cambridge, UK.
- 553 Ruiz, M., Díaz, J., Gallart, J., Pulgar, J.A., González-Cortina, J.M., and López, C.,
554 2006. Seismotectonic constraints at the western edge of the Pyrenees: aftershock
555 series monitoring of the 2002 February 21, 4.1 Lg earthquake. *Geophys. J. Int.*, 166:
556 238–252
- 557 Saccorotti, G., Carmona, E., Ibáñez J. M., and Del Pezzo, E., 2002. Spatial
558 characterization of Agron, southern Spain, 1988-1989 seismic series. *Phys. Earth
559 Planet. Int.*, 129: 13-29.
- 560 Scarfi, L., Langer, H., and Gresta, S., 2003. High-precision relative locations of two
561 microearthquakes clusters in Southeastern Sicily, Italy. *Bull. Seismol. Soc. Am.*, 93:
562 1479-1497.

- 563 Schaff, D.P., and Richards, P.G., 2004. Lg-wave cross correlation and double-
564 difference location: application to the 1999 Xiuyan, China, sequence. *Bull. Seismol.*
565 *Soc. Am.*, 94: 867-879.
- 566 Scherbaum, F. and J. Wendler, 1986. Cross spectral analysis of Swabian Jura (SW
567 Germany) three-component microearthquake recordings. *J. Geophys.* 60, 157-166.
- 568 Serpelloni, E., Vannucci, G., Pondrelli, S., Argnani, A., Casula, G., Anzidei, M.,
569 Baldi, P., and Gasperini, P., 2007. Kinematics of the Western Africa-Eurasia plate
570 boundary from focal mechanisms and GPS data. *Geophys. J. Int.*, in press.
- 571 Smith, K.D. and Priestley, K.F., 2000. Faulting in the 1986 Chalfant, California,
572 Sequence: Local Tectonics and Earthquake Source Parameters, *Bull. Seismol. Soc.*
573 *Am.*, 90, 813-831.
- 574 Stich, D., Alguacil, G., and Morales, J., 2001. The relative locations of the multiplets
575 in the vicinity of the Western Almeria (Southern Spain) earthquake series 1993-1994.
576 *Geophys. J. Int.*, 146: 801-812.
- 577 Stich, D., Ammon, C.J., and Morales, J., 2003. Moment tensor solutions for small and
578 moderate earthquakes in the Ibero-Maghreb region. *J. Geophys. Res.* 108, 2148,
579 doi10.1029/2002JB002057.
- 580 Stich, D., Serpelloni, E., Mancilla, F., and Morales, J., 2006. Kinematics of the
581 Iberia-Maghreb plate contact from seismic moment tensors and GPS observations.
582 *Tectonophysics* 426, 295-317.
- 583 Vidal, F., 1986. Sismotectónica de la Región Béticas-Mar de Alborán. PhD thesis,
584 University of Granada, Granada.

585 Waldhauser, F., and Ellsworth, W.L., 2000. A double-difference earthquake location
586 algorithm: method and application to the Northern Hayward fault, California. Bull.
587 Seismol. Soc. Am., 90: 1353–1368.

588

589

590 **Figure captions**

591

592 Figure 1. Seismicity of S-Spain and surrounding area 1983-2007 ($m \geq 3.5$, Instituto
593 Andaluz de Geofísica). The box in SE-Spain marks the study area where the 2005
594 sequence occurred.

595

596 Figure 2. Map with locations of the main historical events ($I_{\max} > VIII$) – triangles –
597 and instrumental events with magnitude > 4 – circles – that affected the region of
598 Murcia.

599

600 Figure 3. Time-frequency distribution of the 2005 La Paca seismic series. Arrows
601 indicate the initial and final date for analysis in this study (January 29 to February
602 20).

603

604 Figure 4. Single earthquake relocations for 262 earthquakes of the La Paca sequence
605 from January 29 2005 to February 20 2005 (circles, the location of the mainshock is
606 marked by a star). Stations considered for the waveform analysis are represented by
607 triangles while squares indicate the location of some of the villages near the
608 epicentral area.

609

610 Figure 5. Organization of 118 multiplets (45 per cent of the initial data set) into 16
611 clusters with a minimum of 3 members. Further, 20 doublets were obtained but they
612 have not been included in the master relative location procedure.

613

614 Figure 6. Map showing the location of the 16 families with more than 3 members
615 (circles); family numbers according to Fig. 5 have been labelled. Locations have been
616 calculated as the mean location of all individual multiplets included in each of them.
617 The depths of families are in the range 3-18km. The main shock of the seismic series
618 has been represented by a star.

619

620 Figure 7. Example for waveform similarity within a multiplet family (normalized
621 seismograms for cluster no. 3 at station VELZ) showing P- and S-arrivals.

622

623 Figure 8. Precise relative locations of multiplets within three clusters. The
624 corresponding master events are represented by a star at relative coordinates (0,0).
625 Horizontal planes of the 68.3% confidence ellipsoids have been plotted. The chosen
626 examples show predominant average directions of epicentre distributions, of about
627 N145°E (cluster no. 17), N6°E (cluster no. 9) and N40°E (cluster no. 5).

628

629 Figure 9. Map showing the location of the 118 multiplets included in some of the
630 clusters (a) before being relocated and (b) after master relative location. A higher
631 concentration of relocated seismicity can be observed. In both cases main shock has
632 been represented by a star and the locations of some of the main villages near the
633 epicentral area have been indicated by triangles. (c) Map showing the trends of planes

634 fitted to the relocated clusters, with predominant orientations around N145°E and
635 N6°E and N40°E.

636

637 Figure 10. Equiareal projections of the best-fitting planes through relocated multiplet
638 clusters. Clusters number 7, 17, 23, 31 and 36 show epicentre lineaments with an
639 average direction of $N145^{\circ}\pm 17^{\circ}E$. There are also two secondary epicentre lineaments
640 with approximate directions $N6^{\circ}\pm 6^{\circ}E$ and $N40^{\circ}\pm 7^{\circ}E$, which correspond, respectively,
641 to clusters number 8, 9, 21, 28 and 32 and clusters number 3, 4, 5 and 35.

642

643 Figure 11. Plot of function $Q(N,K)$ versus the sliding window length K for the spatio-
644 temporal PCA. The curve becomes near-constant for values of K around 30, and a
645 sliding window of $K=31$ events was selected in this study.

646

647 Figure 12. Temporal evolution of the rupture process modelled by PCA. Equiareal
648 projections of the planes are represented consecutive in time. Three principal
649 directions are found: $N145^{\circ}\pm 3^{\circ}E$ (projections (a), (d) and (k)), $N42^{\circ}\pm 4^{\circ}E$ (projections
650 (b), (e) and (f)) and $N14^{\circ}\pm 4^{\circ}E$ (projections (c), (g) to (i), (l) and (m)).

651

652 Figure 13. Trends of seismicity from multiplet analysis (black solid lines), from PCA
653 analysis (black dotted lines) and trend of nodal planes of moment tensor mechanisms
654 (from Benito et al., 2007, grey solid lines) concentrate along $\sim N10^{\circ}E$, $\sim N40^{\circ}E$ and
655 $\sim N140^{\circ}E$ directions, with opposite sense of slip, showing the simultaneous activity of
656 conjugate strike-slip faults. The regional maximum stress direction (grey arrows,
657 from Stich et al., 2006) is consistent with local deformation.

658

659

660 **Tables**

661

662 Table 1. Best fitting planes through relocated multiplet clusters.

Cluster number	Number events	Azimuth (°)	Dip(°)
3	7	41	83
4	3	44	83
5	7	30	88
7	3	153	89
8	4	6	87
9	10	12	86
13	3	114	86
17	25	126	87
20	9	64	88
21	4	177	87
23	23	163	86
28	3	177	88
31	7	155	86
32	3	7	88
35	3	40	87
36	4	144	89

663

664

665 Table 2. Planes characterizing temporal evolution of rupture process.

666 NCP indicates the number of time consecutive planes used in the construction of the
 667 average plane and gives an idea of its relative importance. Other columns represent
 668 azimuth and dip values of the plane as well as spatial location (longitude, latitude and
 669 depth) of the ellipsoid.

PCA						
Plane	NCP	Azimuth (°)	Dip(°)	Long (°)	Lat (°)	Depth (km)
(a)	2	144	60	-1.785	37.821	10.0
(b)	2	44	70	-1.790	37.823	10.2
(c)	4	11	44	-1.792	37.824	10.1
(d)	5	147	35	-1.797	37.825	10.3
(e)	2	49	73	-1.807	37.827	10.5
(f)	5	39	84	-1.807	37.827	10.4
(g)	2	6	80	-1.807	37.827	10.0
(h)	2	9	89	-1.806	37.825	9.5
(i)	2	16	11	-1.803	37.829	9.3
(j)	4	173	88	-1.802	37.828	9.3
(k)	3	141	88	-1.799	37.827	8.9
(l)	12	17	90	-1.799	37.825	8.7
(m)	4	13	76	-1.793	37.822	8.4

670

671

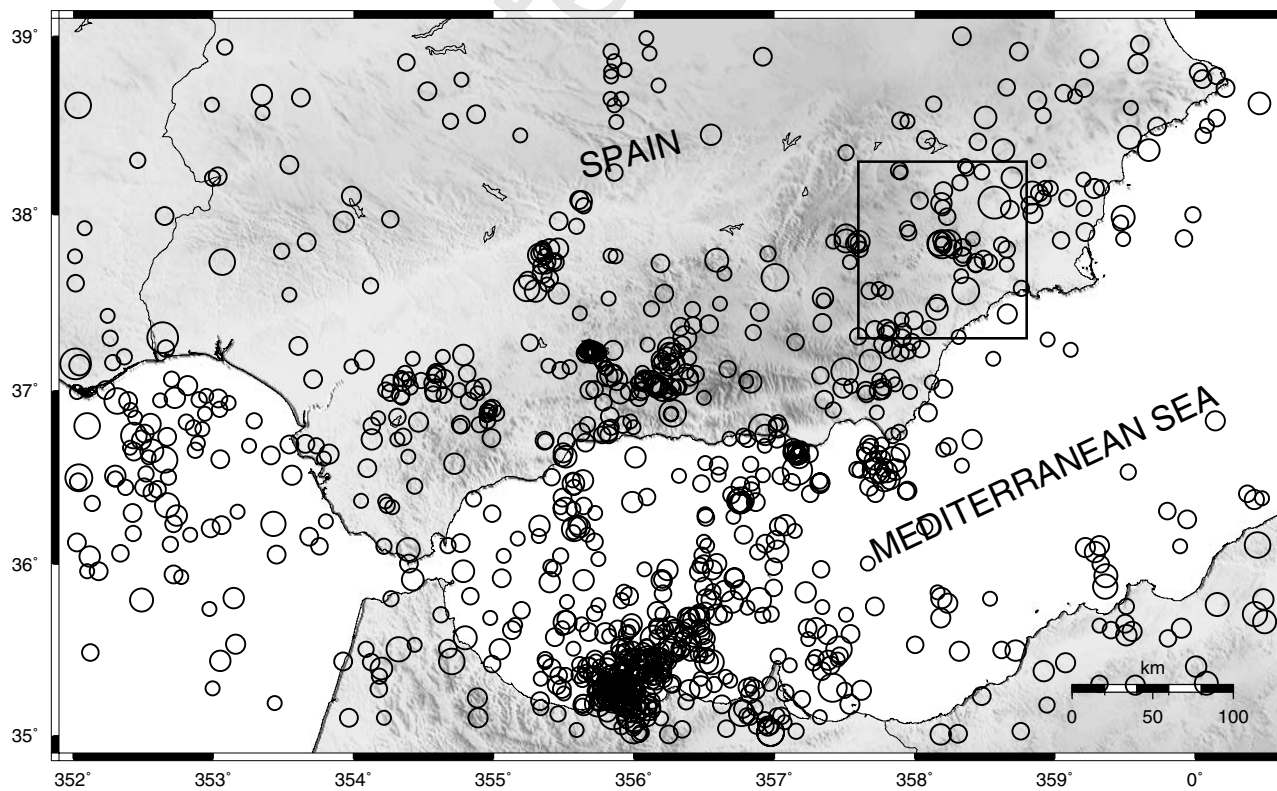
672 Table 3. Moment tensor solutions for the 2005 La Paca earthquake and the two
 673 largest aftershocks (from Stich et al., 2006, Benito et al., 2007). The double-couple
 674 component is represented by fault angle parameters for the two nodal planes. The

675 non-double-couple remainder (CLVD) is given in percent. M_0 is the seismic moment
 676 and M_w the moment magnitude.

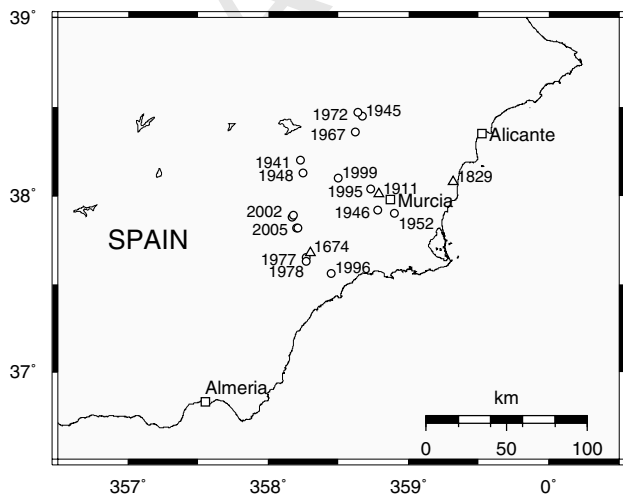
Date	time	fault angle parameters	clvd	M_0 [Nm]	M_w
y/ m/ d		(strike/ dip/ rake)	[%]		
2005/01/29	07:41:31	132/ 85/ -153; 40/ 63/ -5	3	$1.62 \cdot 10^{16}$	4.8
2005/02/03	11:40:33	110/ 84/ -136; 15/ 46/ -7	6	$2.44 \cdot 10^{15}$	4.2
2005/02/04	01:09:41	109/ 82/ -136; 11/ 47/ -10	3	$8.65 \cdot 10^{14}$	3.9

677

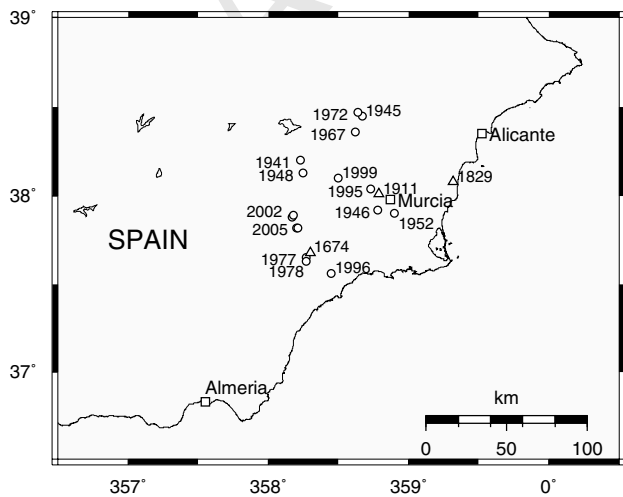
Accepted Manuscript

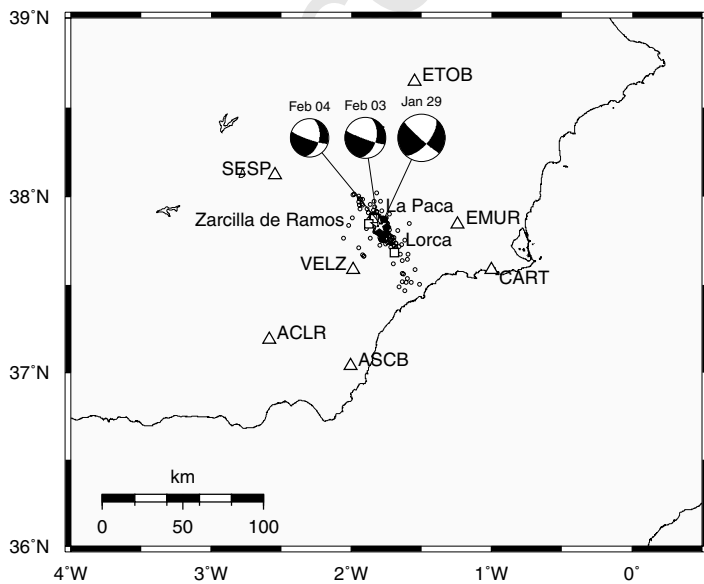


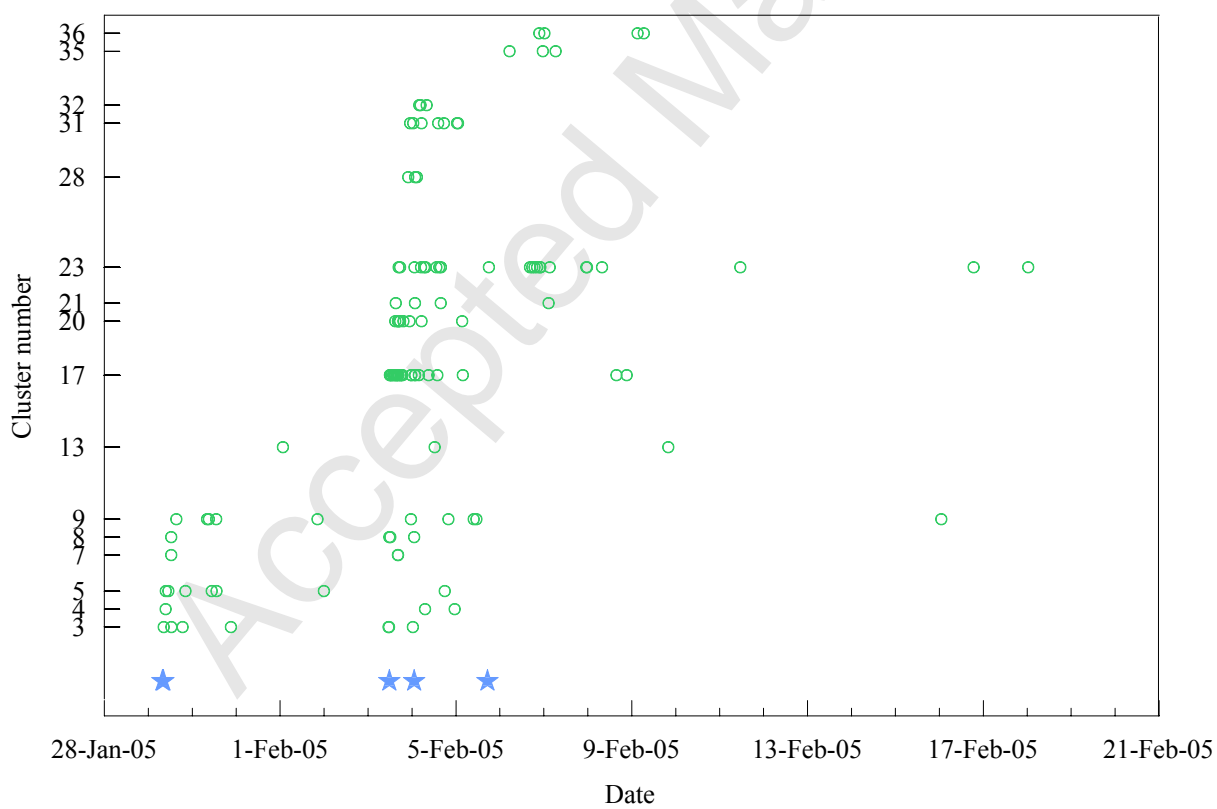
Accepted Manuscript



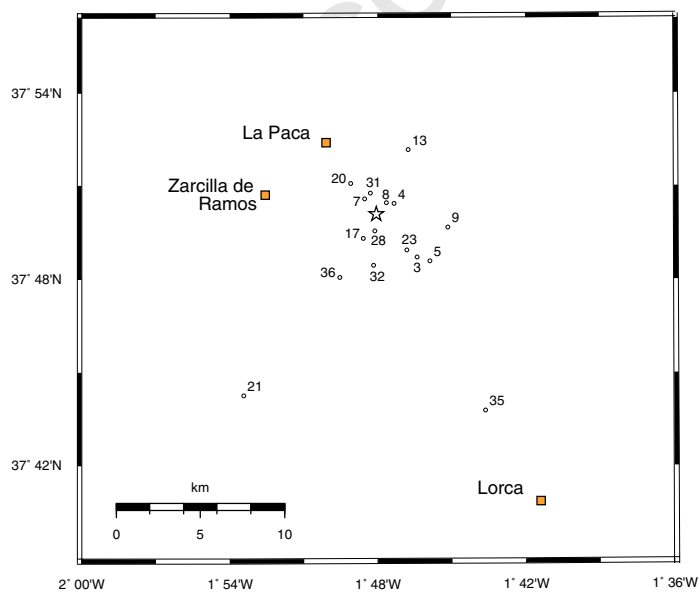
Accepted Manuscript

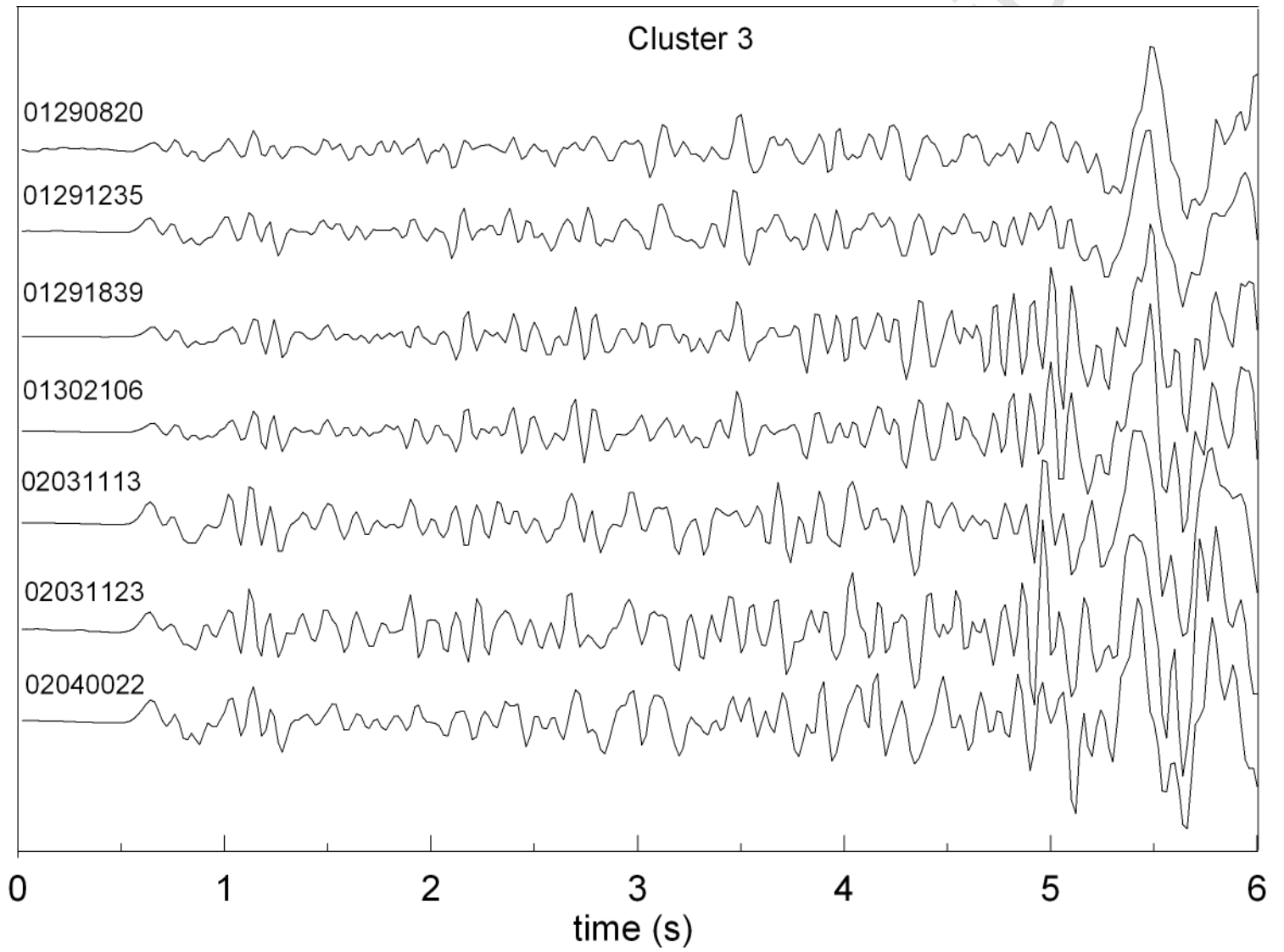


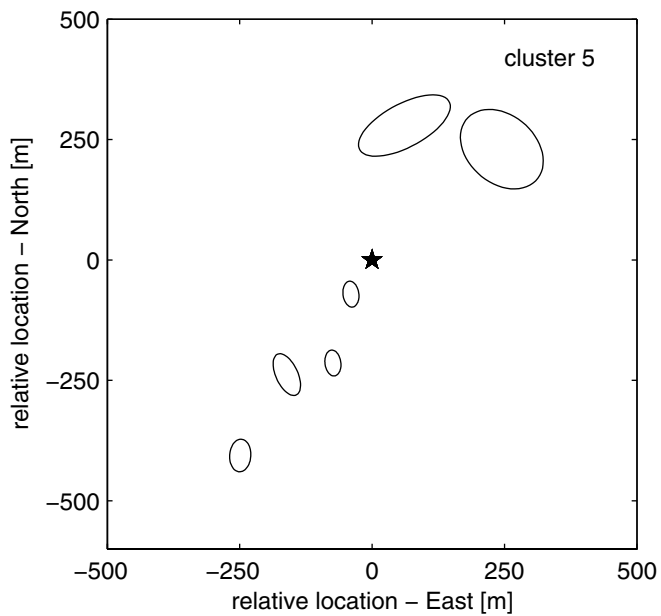
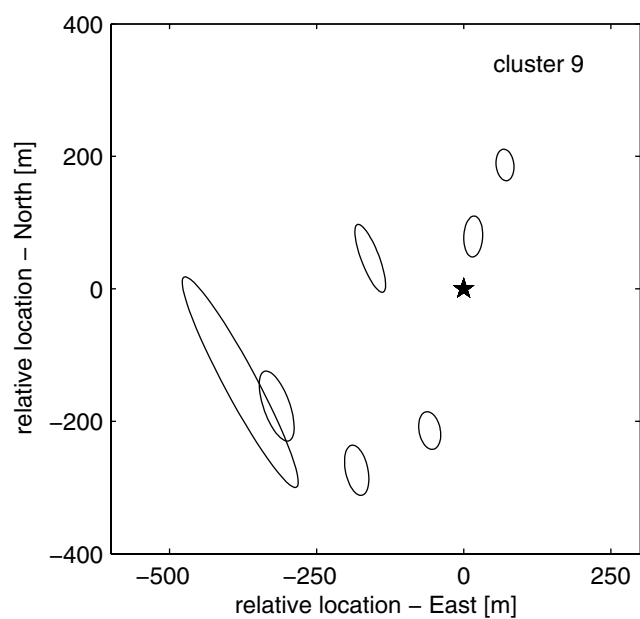
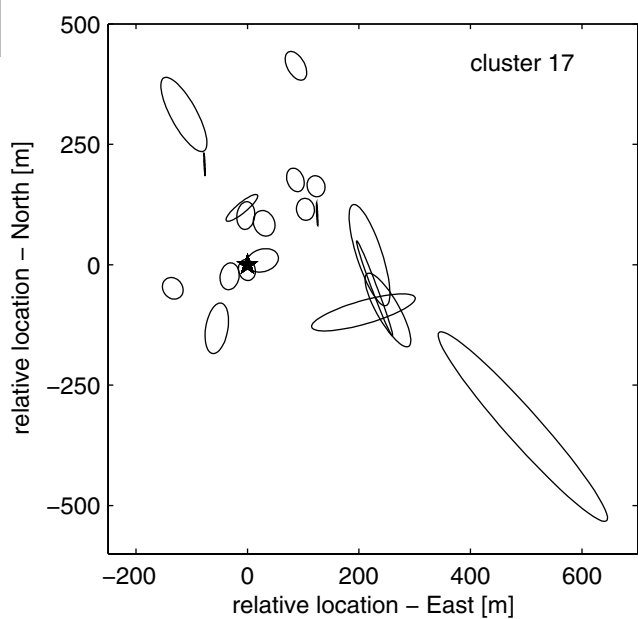


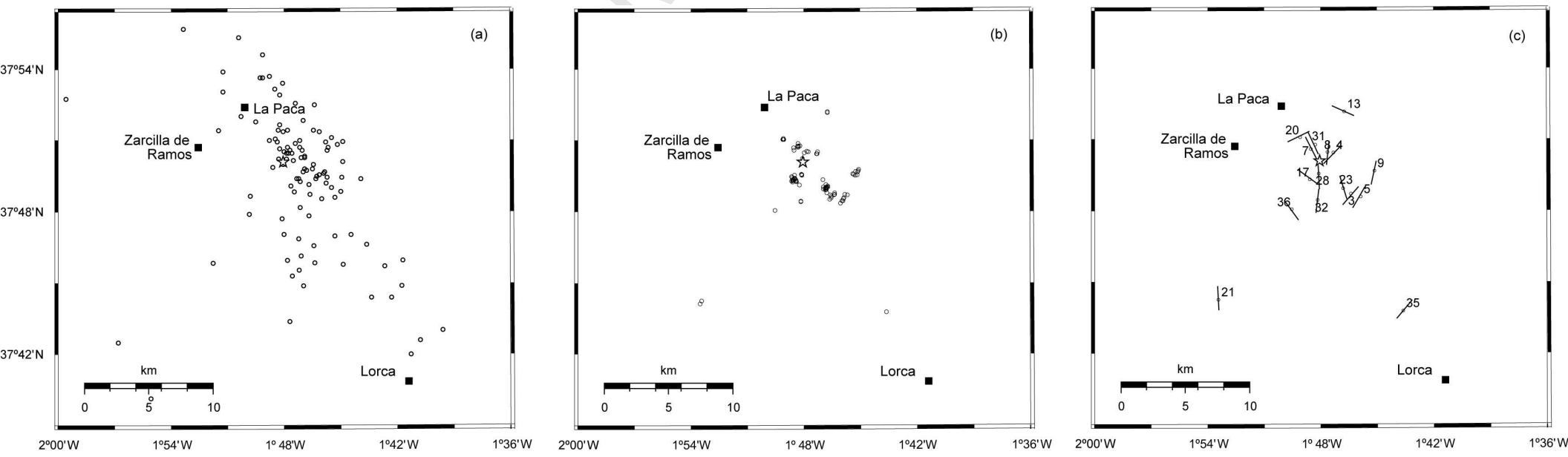


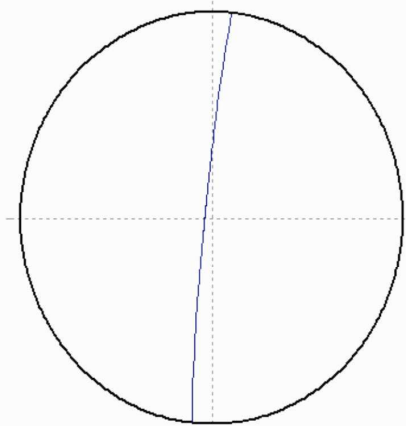
Accepted Manuscript



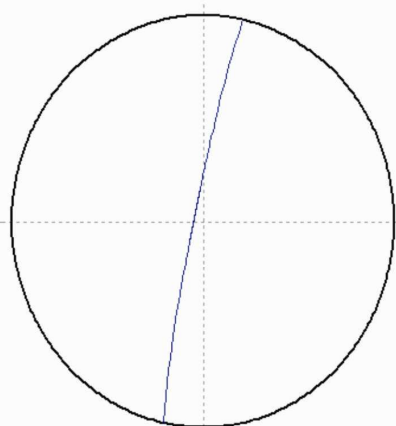




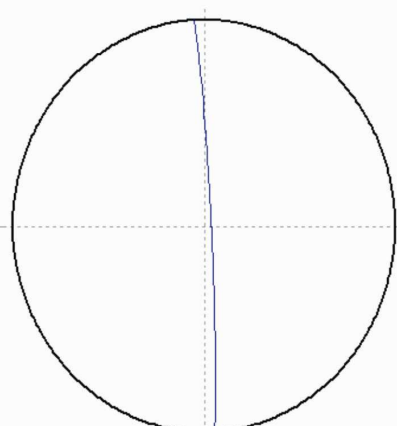




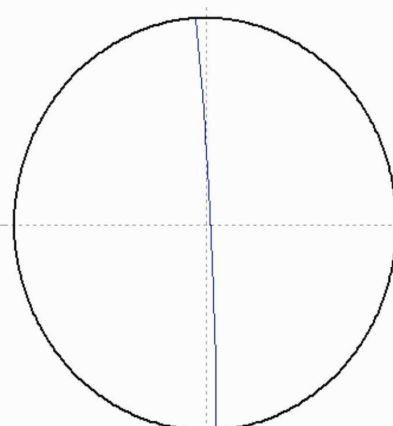
cluster 8



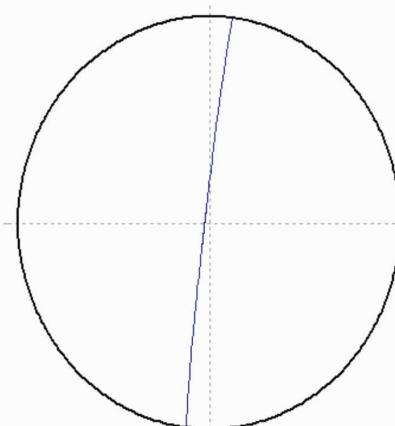
cluster 9



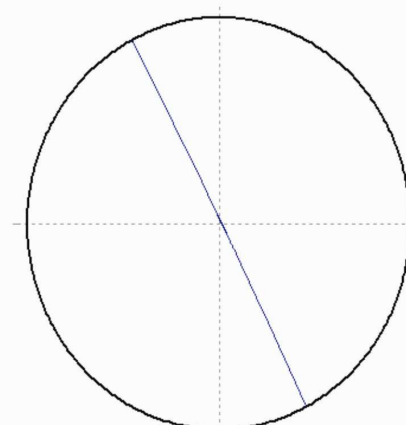
cluster 21



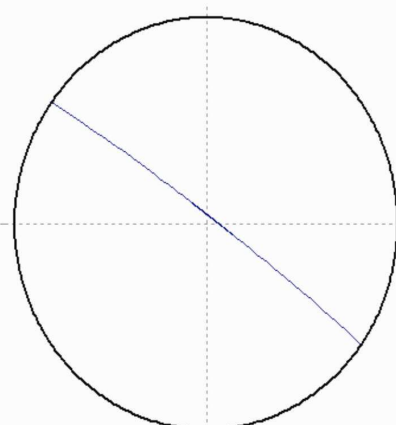
cluster 28



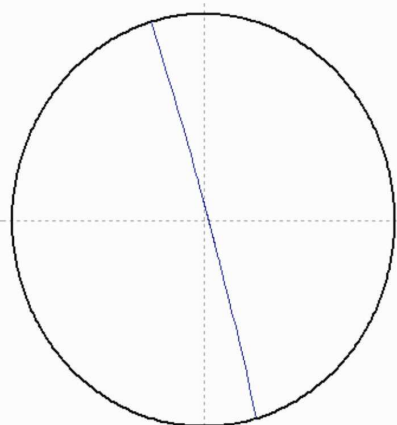
cluster 32



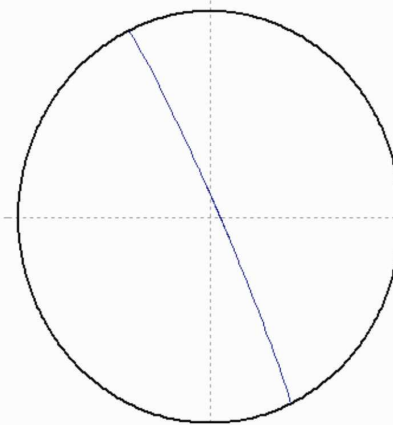
cluster 7



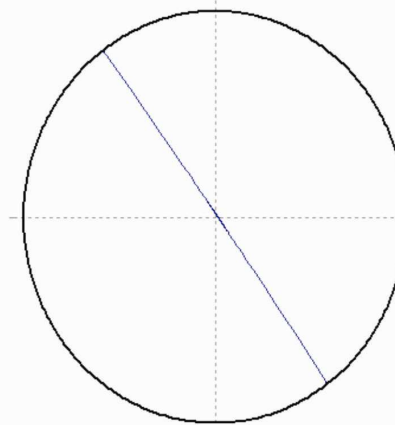
cluster 17



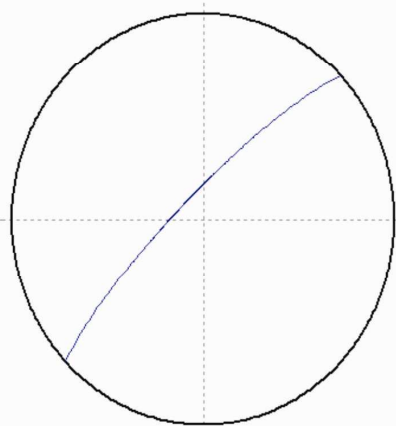
cluster 23



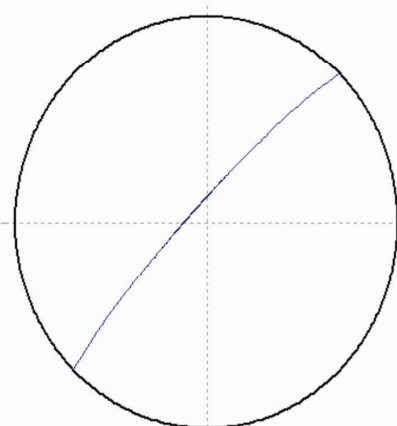
cluster 31



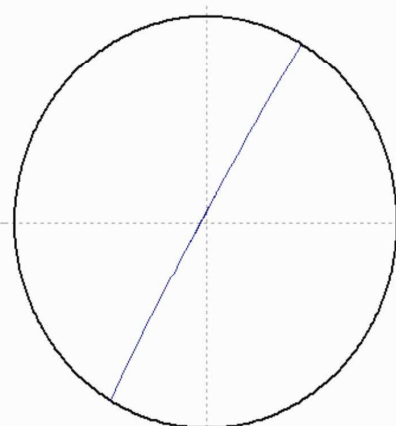
cluster 36



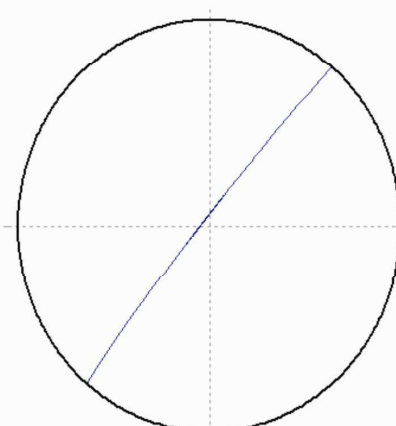
cluster 3



cluster 4



cluster 5



cluster 35

